KKU SCIENCE JOURNAL
Journal Home Page : https://ph01.tci-thaijo.org/index.php/KKUSciJ
Published by the Faculty of Science, Khon Kaen University, Thailand

การสังเคราะห์อนุภาคนาโนเงินจากสารสกัดใบมะกรูดเพื่อการย่อยสลายสีย้อมคริสตัลไวโอเลต

Synthesis of Silver Nanoparticles from Kaffir Lime Leaf Extract for Crystal Violet Dye Degradation

ณัฐวิศิษฏ์ ยะสารวรรณ[1*]

Nuttawisit Yasarawan[1*]

[1]ภาควิชาเคมี คณะวิทยาศาสตร์ มหาวิทยาลัยบูรพา จังหวัดชลบุรี 20130

[1]Department of Chemistry, Faculty of Science, Burapha University, Chonburi, 20130, Thailand

บทคัดย่อ

งานวิจัยนี้นำเสนอการสังเคราะห์อนุภาคนาโนเงิน (AgNPs) ด้วยวิธีที่เป็นมิตรต่อสิ่งแวดล้อมโดยใช้สารสกัดจากใบมะกรูด (KLLE) เป็นตัวรีดิวซ์และสารเพิ่มความเสถียร ทั้งยังศึกษาอิทธิพลของปัจจัยต่าง ๆ ที่มีต่อการสังเคราะห์ ได้แก่ ความเข้มข้นของ $AgNO_3$ ร้อยละของ KLLE อุณหภูมิ และ pH โดยพบว่าสภาวะที่เหมาะสม (55°C 20 mM $AgNO_3$ 20% KLLE และ pH ~7) ทำให้เกิด AgNPs ทรงกลมที่มีขนาดเส้นผ่านศูนย์กลางเฉลี่ย 7.5 ± 1.9 nm ประสิทธิภาพของ AgNPs ในฐานะตัวเร่งปฏิกิริยาเชิงแสงถูกประเมินจากความสามารถในการเร่งการย่อยสลายสีย้อมคริสตัลไวโอเลต (CV) ภายใต้แสงขาวจากหลอด LED และแสงอาทิตย์ โดยพบว่าปฏิกิริยาซึ่งถูกเร่งด้วย AgNPs เป็นไปตามแบบจำลองจลนศาสตร์อันดับหนึ่ง การฉายแสงจากหลอด LED เป็นเวลา 12 ชั่วโมงให้ค่าการกำจัด CV สูงสุดที่ 89% ในขณะที่การรับแสงอาทิตย์เป็นเวลาเพียง 6.5 ชั่วโมงสามารถกำจัด CV ได้ในระดับที่ใกล้เคียงกันคือ 85% ผลลัพธ์เหล่านี้แสดงถึงศักยภาพของ AgNPs ที่สังเคราะห์จาก KLLE ในการเป็นตัวเร่งปฏิกิริยาเชิงแสงที่มีประสิทธิภาพสำหรับการบำบัดมลพิษทางสิ่งแวดล้อม

ABSTRACT

This study presents a green synthesis method for silver nanoparticles (AgNPs) using kaffir lime leaf extract (KLLE) as a natural reductant and stabilizer. Influence of synthesis parameters, including $AgNO_3$ concentration, KLLE percentage, temperature, and pH was investigated. Optimal conditions (55°C, 20 mM $AgNO_3$, 20% KLLE and pH ~7) led to the formation of spherical AgNPs with an average diameter of 7.5 ± 1.9 nm. The photocatalytic performance of AgNPs was evaluated through crystal violet (CV) dye degradation under white light from an LED bulb and sunlight. The degradation catalyzed by AgNPs followed first-order kinetics. LED irradiation for 12 hours resulted in a maximum CV removal of 89%, whereas sunlight exposure for only 6.5 hours achieved a comparable CV removal of 85%. These findings highlight the potential of KLLE-derived AgNPs as efficient photocatalysts for environmental remediation.

*Corresponding Author, E-mail: nuttawisit@go.buu.ac.th

Received date: 5 May 2025 | Revised date: 27 August 2025 | Accepted date: 29 August 2025

doi: 10.14456/kkuscij.2025.35

คำสำคัญ: การสังเคราะห์สีเขียว อนุภาคนาโนเงิน ตัวเร่งปฏิกิริยาเชิงแสง การย่อยสลายสีย้อม
Keywords: Green Synthesis, Silver Nanoparticles, Photocatalysts, Dye Degradation

INTRODUCTION

Silver nanoparticles (AgNPs) are widely studied for their biomedical applications and, more recently, for their photocatalytic activity. Previous studies have shown that AgNPs and their composites efficiently degrade organic dyes under light irradiation (Marimuthu *et al*., 2020). The photocatalytic degradation process can operate without harmful chemicals, such as oxidative bleaching agents, thereby significantly reducing its environmental impact. Upon excitation by incident light, collective oscillations of electron density localized on the AgNP surfaces, known as surface plasmons, transfer energy to the conduction electrons. These excited electrons interact with oxygen and water to generate reactive oxygen species (ROS), such as superoxide and hydroxyl radicals, which degrade dye molecules into non-toxic products (Marimuthu *et al*., 2020). Conventional AgNP synthesis methods often employ hazardous chemical reductants, such as borohydride, hydrazine, and dimethylformamide, prompting significant interest in greener, biogenic reductants (Gebre, 2023). Plant extracts rich in phenolic compounds, including flavonoids, exhibit bifunctional properties, reducing Ag^{+} to Ag^{0} and sterically stabilizing the resulting colloidal AgNPs. The transfer of electrons from the hydroxyl groups of flavonoids to Ag^{+} ions results in deprotonation and conversion of their molecular structures into quinones, which bind firmly to the AgNP surfaces (Gebre, 2023).

This research aims to present a simple and safe method for synthesizing colloidal AgNPs based on the reaction between silver ions and kaffir lime leaf extract (KLLE). Kaffir lime (*Citrus hystrix* DC) is a citrus plant of considerable economic importance in Southeast Asia. Its leaves possess a distinct flavor and aroma and have long been utilized in culinary and cosmetic applications. Moreover, kaffir lime is a rich source of flavonoids, particularly hesperidin, rutin, and diosmin (Kanes *et al*., 1993). Notably, Sahu and colleagues reported the successful synthesis of AgNPs using high-purity commercial-grade hesperidin (Sahu *et al*., 2016). Owing to its wide availability in Thailand, low cost, and safety, kaffir lime is therefore a promising natural source of flavonoids for the green synthesis of AgNPs. The effects of synthesis conditions including temperature, silver ion concentration, KLLE percentage, and pH were investigated.

Crystal violet (CV), a water-soluble organic dye used in laboratory and industrial applications (Sana *et al*., 2022), is considered a significant organic pollutant in wastewater due to its high toxicity and carcinogenicity (Mirza and Ahmad, 2020). Consequently, the removal of CV is of great importance for wastewater pollution control. In this study, the AgNPs synthesized were further evaluated for their photocatalytic activity in degrading CV dye under both white LED light and natural sunlight. The results demonstrate that KLLE-derived AgNPs are effective photocatalysts with considerable potential for application in light-driven wastewater treatment.

MATERIALS AND METHODS

1. Materials

Silver nitrate (99.9% Pure PA grade, POCH), crystal violet dye ($C_{25}H_{30}ClN_3$, 96% AR grade, QRëC), methanol (99.8% AR grade, QRëC), ethanol (99.9% AR grade, RCI Labscan) and acetone (99.5%, AR grade, QRëC). Fresh kaffir lime leaves from a local farm in Phra Nakhon Si Ayutthaya province, Thailand.

2. Characterization Methods and General Procedures

UV-Vis spectra were recorded using an Agilent Cary 3500 spectrophotometer, while Fourier-transform infrared (FTIR) spectra were obtained with a Perkin-Elmer System 2000 FTIR spectrometer. X-ray diffraction (XRD) measurement was carried out using a Bruker D2 Phaser diffractometer to examine the crystalline structure of AgNPs. Silver content in AgNPs was determined via X-ray fluorescence (XRF) spectroscopy using a Horiba XGT-9000 system. Particle morphology was characterized using a Philips Tecnai 20 transmission electron microscope (TEM) and a LEO 1450VP scanning electron microscope (SEM) equipped with an energy-dispersive X-ray (EDX) system. In all cases, unless otherwise specified, particle separation from suspensions was carried out by centrifugation at 10,000 rpm for 10 minutes using a Sorvall LYNX 4000 centrifuge.

3. Preparation of KLLE

Approximately 400 g of fresh kaffir lime leaves were washed with tap and deionized (DI) water, then air-dried at room temperature overnight. After drying in an oven at 50ºC for 8 h, the leaves yielded approximately 110 g of dried material, corresponding to a dried yield of 27.5%. The dried leaves were then ground into small pieces using a DXFILL DXM-300 grinding machine. The ground leaves were mixed with 2 L of DI water and stirred at 50ºC for 2 h. The resulting mixture was subsequently filtered to obtain the amber-colored KLLE.

4. Synthesis of AgNPs

A 25 mM $AgNO_3$ stock solution was prepared in DI water. A known volume (9 - 60 mL) of this solution was mixed with KLLE (1.5 - 15 mL) in a conical flask and diluted to 75 mL with DI water. The pH was adjusted dropwise using 0.01 M HNO_3 or NaOH. The mixture was stirred and incubated at 44 - 63ºC using a thermostatted stirrer to form colloidal AgNPs. Aliquots of 1.5 mL were withdrawn from the mixture at specific reaction times to monitor the evolution of the surface plasmon resonance (SPR) band of AgNPs via UV-Vis spectral measurement, and the SPR absorbance increase was fitted to a first-order kinetic model (Kumar *et al*., 2022):

$$A_t = A_\infty - (A_\infty - A_0)e^{-k_f t} \quad (1)$$

where A_t, A_∞ and A_0 represent the absorbance for the SPR band of AgNPs at the incubation time t, at infinite time, and at time zero, respectively. The formation rate constants (k_f) were determined using a non-linear fitting approach.

5. Preparation of Photocatalytic AgNPs

2 L of 25 mM $AgNO_3$ (5.39 g Ag^+) was mixed with 0.5 L of KLLE, yielding a mixture containing 20 mM Ag^+ and 20% KLLE. The mixture was stirred and incubated at 55ºC for 180 min, forming a reddish-brown colloidal AgNP suspension. After cooling, the suspension was centrifuged to remove residual KLLE, and the precipitate was washed twice with DI water to obtain water-washed AgNPs (WW-AgNPs). Dried WW-AgNPs were sticky due to excess organic residues. To remove these residues, WW-AgNPs underwent successive washing cycles with methanol, ethanol, and

acetone. In each cycle, 5 g of WW-AgNPs were redispersed in 25 mL of the respective solvent per centrifuge tube, followed by 20-min ultrasonication, centrifugation, and removal of the supernatant. The final precipitate was air-dried, ground into a fine powder, and designated as OW-AgNPs (organic solvent-washed AgNPs) for use as the photocatalyst. A total of 3.43 g of OW-AgNPs (Ag^0) were obtained, corresponding to a yield of ~64%.

6. Experimental Procedure for Photocatalytic Degradation of CV

Photocatalytic degradation of CV under visible light was performed in a chamber (Figure 1a) equipped with a 25 W white light (WL) LED (Ultra-X, BEC). OW-AgNP powders (40 - 50 mg) were mixed with 200 mL of CV solution (4 - 6 mg L^{-1}) in a beaker. The mixture was stirred in the dark for 1 h to allow dye adsorption, then irradiated by switching on the LED. A small portion was withdrawn from the mixture at specific time interval for UV-Vis spectral measurement. For solar irradiation, the sample was exposed to sunlight in Chonburi, Thailand, from 9:30 AM to 4:00 PM on December 23, 2024. Figure 1b-c shows the total visible photon fluxes from the 25 W WL LED and sunlight, measured using a Thorlabs PM100D optical power meter. In both cases, red photons were predominant (30 - 38%), followed by green and violet photons, but sunlight delivered much higher intensity across the visible spectrum than the LED. The CV absorbance decrease was fitted to a first-order kinetic model:

$$A_t = A_\infty + (A_0 - A_\infty)e^{-k_d t} \quad (2)$$

where A_t, A_∞ and A_0 represent the CV peak absorbance at the irradiation time t, at infinite time, and at time zero, respectively. The degradation rate constant (k_d) was obtained using a non-linear fitting approach. The CV removal percentage (%R), representing degradation efficiency, was calculated as:

$$\%R = \frac{A_0 - A}{A_0} \times 100 \quad (3)$$

where A_0 and A are the peak absorbances of the initial and irradiated CV solutions, respectively.

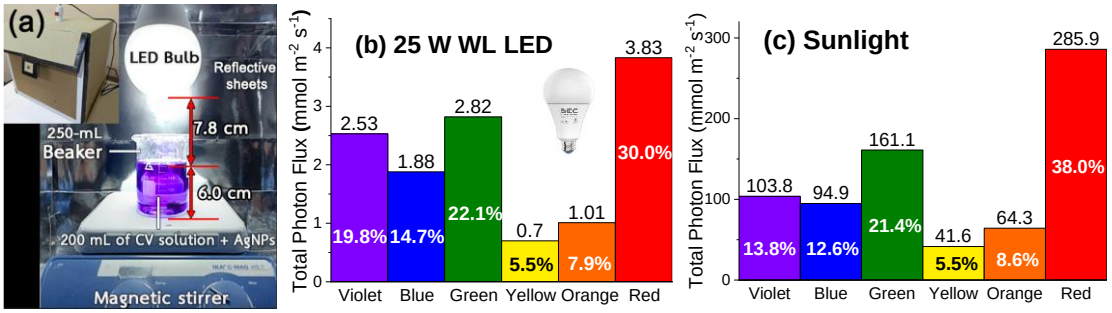

Figure 1 (a) Irradiation chamber: exterior and interior views showing photocatalytic setup. (b-c) Total visible photon fluxes from (b) 25 W white light LED in the chamber and (c) sunlight.

RESULTS AND DISCUSSION

1. Effect of Temperature on AgNP Formation

At 27 ± 2ºC, no AgNP formation was observed in the mixture containing 20 mM $AgNO_3$ and 20% KLLE after 12 h of incubation, as confirmed by UV-Vis spectroscopy and visual inspection. However, incubation at 55ºC caused the mixture's color to change from yellow to reddish-brown within 45 - 180 minutes (Figure 2a),

corresponding to the development of the SPR band of AgNPs at ~470 nm. (Figure 2b). The time-dependent increase in SPR absorbance followed first-order kinetics (Figure 2c), with the rate constants provided in Table 1.

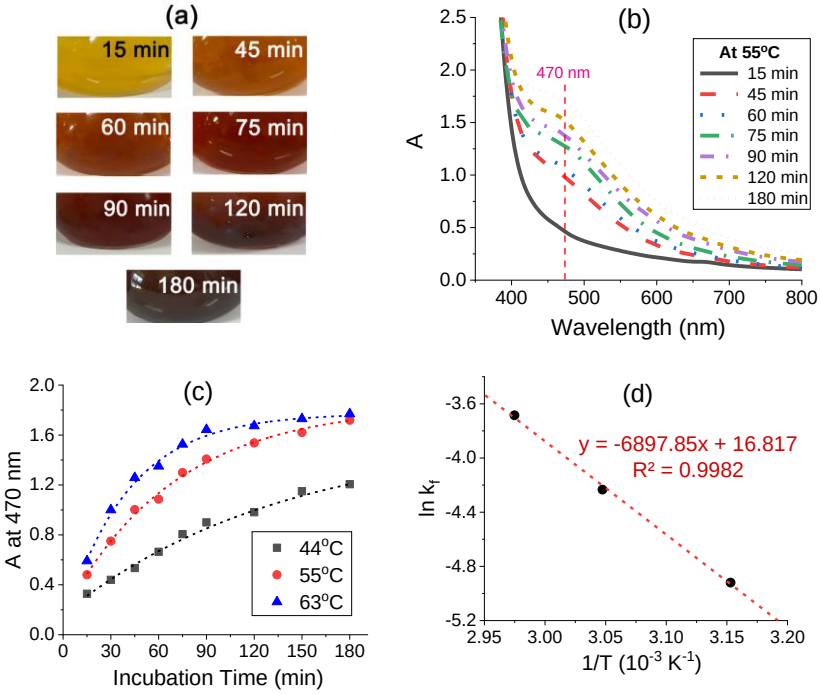

Figure 2 (a) Color change of the mixture containing 20 mM $AgNO_3$ and 20% KLLE during incubation at 55°C. (b) UV–Vis spectra of the mixture at various incubation times. (c) First-order kinetic plot of the SPR absorbance increase at various temperatures. (d) The Arrhenius plot for the AgNP formation.

Table 1 Rate constants (k_f) and goodness-of-fit parameters for AgNP formation at different temperatures.

Temperature (°C)	k_f (min^{-1})	Chi^2	R^2
44	0.0073 ± 0.0003	0.0029	0.9829
55	0.0145 ± 0.0019	0.0018	0.9943
63	0.0251 ± 0.0023	0.0013	0.9955

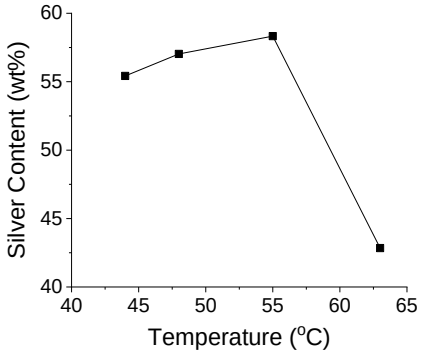

Figure 3 Silver content in WW-AgNPs as determined by EDX analysis at various synthesis temperatures.

The slope of the Arrhenius plot (Figure 2d) indicated an activation energy of 13.7 kcal mol^{-1}, comparable to the reported value for Ag^{+} reduction by ascorbic acid (10.6 kcal mol^{-1}) (Mushran *et al*., 1974), suggesting that Ag^{+} reduction by KLLE could be the rate-determining step in AgNP formation. According to EDX analysis (Figure 3), the Ag content in WW-AgNPs increased with temperature, reaching the maximum of 58 wt% at 55ºC before dropping to 43 wt% at 63ºC, suggesting that 55ºC was optimal for silver incorporation. The decline in Ag content at 65ºC may result from the thermal degradation of bioactive compounds in KLLE or reduced particle stability.

2. Effect of $AgNO_3$ Concentration, KLLE Percentage and pH on AgNP Formation

Figure 4a shows that at 55ºC and 180 minutes of incubation, the AgNP SPR absorbance at 470 nm increased with $AgNO_3$ concentration up to 16 mM, after which KLLE became a limiting factor. Figure 4b shows a steady increase in absorbance with increasing KLLE percentage. Figure 4c reveals a sharp absorbance increase from pH 3 to 7. Since cloudy white AgOH precipitates formed at pH values above 7, AgNP formation was most favorable under neutral conditions.

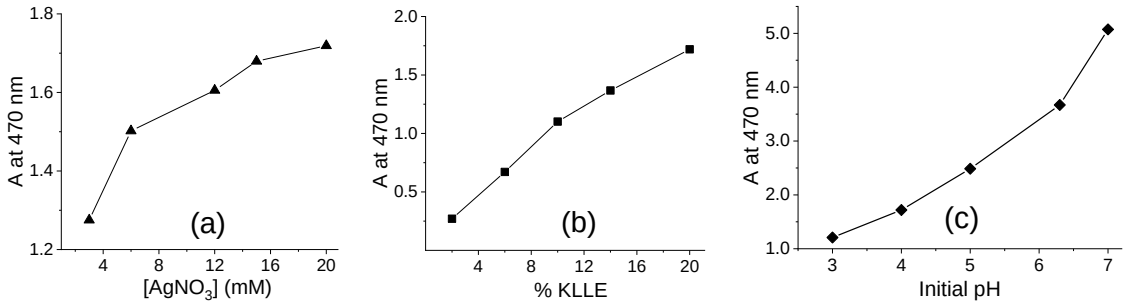

Figure 4 SPR absorbance of AgNPs versus (a) [$AgNO_3$] with %KLLE = 20, (b) %KLLE with [$AgNO_3$] = 20 mM, and (c) initial pH with [$AgNO_3$] = 20 mM and %KLLE = 20. All reactions were conducted at 55ºC for 180 minutes.

3. FTIR and UV-Vis Spectroscopic Analysis of KLLE and KLLE-Derived AgNPs

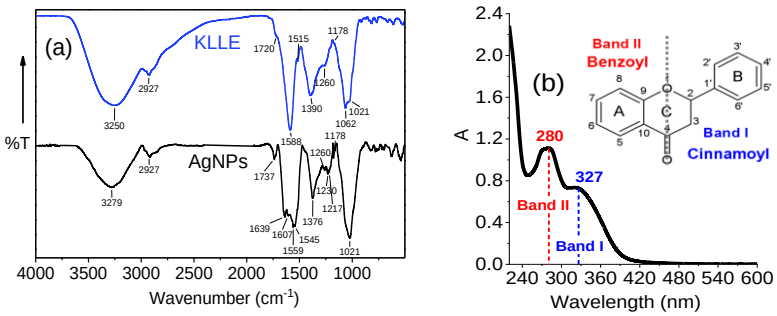

Figure 5 (a) FTIR spectra of air-dried KLLE and WW-AgNPs synthesized at 55ºC. (b) UV-Vis spectrum of 1% KLLE, with an inset showing benzoyl and cinnamoyl moieties in a typical flavonoid backbone.

Comparative FTIR analysis of KLLE and biogenic AgNPs provides insight into the role of bioactive compounds during nanoparticle synthesis. Figure 5a shows the FTIR spectra of air-dried KLLE and KLLE-derived AgNPs after water washing (WW-AgNPs). The O-H stretching band shifted from 3250 cm^{-1} in KLLE to 3279 cm^{-1} in

AgNPs with reduced intensity, suggesting a decrease in phenolic OH groups due to oxidation and possible interaction with Ag. Similarly, quercetin has shown blue-shifted OH stretching band upon interacting with silica particles (Catauro *et al*., 2015). A new band at 1737 cm^{-1} suggests C=O stretching of quinonoid structures, implying flavonoid oxidation. The phenolic O-H bending band shifted from 1390 cm^{-1} in KLLE to 1376 cm^{-1} in AgNPs, with a relative weakening relative to the C-O stretching band at 1021 cm^{-1}, implying partial loss of phenolic OH groups and binding to AgNP surfaces. New peaks at 1545 - 1639 cm^{-1} can be attributed to conjugated C=O and aromatic C=C stretching vibrations, which may indicate the possible transformation of flavonoids into quinone-like structures. The UV-Vis spectrum of KLLE (Figure 5b) showed two characteristic flavonoid absorption bands: Band II at 280 nm (associated with ring A) and Band I at 327 nm (associated with ring B). These bands resemble those reported for hesperidin in the literature (Gattuso *et al*., 2007), but the marked intensity and broadening of Band I suggests the presence of other flavonoids, possibly rutin (band I at ~360 nm) (Qi *et al*., 2015) and diosmin (band I at ~340 nm) (Srilatha *et al*., 2013), with a C2 = C3 bond that enhances electron delocalization in the cinnamoyl moiety.

4. Morphology and Crystalline Phases of Photocatalytic AgNPs

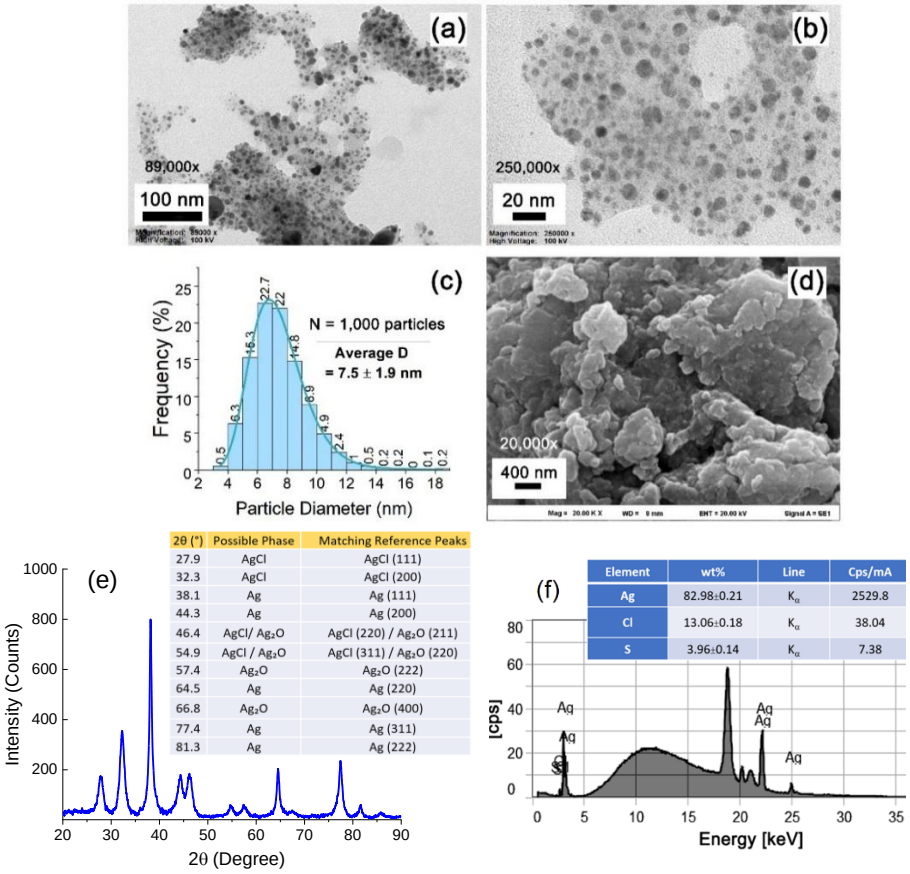

Figure 6 (a - b) TEM images of OW-AgNPs synthesized at 55ºC, at different magnifications: (a) 89,000× and (b) 250,000×. (c) Particle size distribution derived from TEM analysis. (d) SEM image of OW-AgNPs at 20,000× magnification. (e) XRD pattern of OW-AgNP powders, with peak assignments included. (f) XRF emission spectrum of OW-AgNP powders, with elemental analysis data included.

The TEM images (Figure 6 a - b) show that OW-AgNPs have a pseudo-spherical morphology with an average diameter of 7.5 ± 1.9 nm (Figure 6c). The SEM image (Figure 6d) provides limited morphological details due to lower resolution but reveals a smooth surface, possibly indicating organic coverage. Figure 6e shows the XRD pattern of AgNPs (OW-AgNPs) synthesized at 55°C. Peaks at 2θ values of 38.1°, 44.3°, 64.5°, 77.4°, and 81.3° correspond to the FCC Ag lattice (COD 1100136). Other peaks likely indicate the presence of Ag_2O (cubic, COD 1010486) and AgCl (FCC, COD 9008597). The formation of Ag_2O was common for AgNPs synthesized in air under heating. Chloride ions in KLLE likely led to AgCl formation, as supported by XRF data (Figure 6f) showing ~13 wt% Cl. A small sulfur content (~4 wt%) could be due to organosulfur compounds in KLLE.

5. Photocatalytic Performance of AgNPs in the Degradation of CV

In the absence of AgNPs, CV degradation was well described by the zero-order kinetic model ($A_t = A_0 - k_d t$), whereas the AgNP-catalyzed process adhered to first-order kinetic model (Equation 2). The degradation rate constants (k_d) and the CV removal percentages (%R) under various conditions are summarized in Table 2. At an initial [CV] of 4 mg L^{-1} and a catalyst dose of 0.20 g L^{-1}, sunlight exhibited superior photocatalytic performance, yielding k_d of 0.3922 ± 0.0492 h^{-1} and 85% CV removal after 6.5 h of irradiation. In comparison, using the WL LED under identical conditions resulted in a lower k_d of 0.1815 ± 0.0167 h^{-1} and a lower CV removal of 76% after 6.5 h. The higher CV removal under sunlight than under white LED light is likely due to its greater photon flux (Figure 1). Our KLLE-derived AgNPs achieved sunlight-driven CV removal comparable to TiO_2 powders (76 - 81% in 5 h) (Brandão *et al*., 2025), whereas AgNPs from radish microgreen and *Clerodendrum infortunatum* leaf extracts showed higher removal (97% and 95%) due to higher catalyst doses (Ashkar *et al*., 2023; Mandal *et al*., 2024).

Table 2 Rate constants (k_d), goodness-of-fit parameters and CV removal percentage (%R) for the photocatalytic degradation of CV under different conditions.

Light Source	Initial [CV] (mg L^{-1})	Catalyst Dose (g L^{-1})	k_d (h^{-1})	Chi^2	R^2	%R
25W WL LED	4	0	0.0049 ± 0.0002	3.57×10^{-6}	0.9901	11% (6.5 h) 15% (12 h)
		0.20	0.1815 ± 0.0167	3.05×10^{-6}	0.9957	76% (6.5 h) 83% (12 h)
		0.25	0.2265 ± 0.0101	2.45×10^{-6}	0.9987	81% (6.5 h) 89% (12 h)
	6	0.20	0.3411 ± 0.0293	2.54×10^{-6}	0.9941	81% (6.5 h) 87% (12 h)
Sunlight	4	0.20	0.3922 ± 0.0492	6.29×10^{-6}	0.9986	85% (6.5 h)

Figure 7 (a - b) displays the UV-Vis spectra of CV solutions (4 mg L^{-1}) under WL irradiation. Without AgNPs (Figure 7a), the CV absorption peak at 590 nm decreased only slightly, indicating minimal photodegradation. In contrast, the presence of catalytic AgNPs (Figure 7b) resulted in a pronounced decline in the peak absorbance over time. Figure 7c presents the increase in CV removal percentage over time at two different AgNP doses (0.20 and 0.25 g L^{-1}), with an initial [CV] of 4 mg L^{-1} under WL irradiation. The uncatalyzed system exhibited minimal dye removal (~15% after 12 h), while increasing the AgNP dose from 0.20 to 0.25 g L^{-1} significantly enhanced removal efficiency, improving from 83%

to 89% after 12 h. Figure 7d further shows that, at a fixed AgNP dose of 0.20 g L^{-1}, increasing the initial [CV] from 4 to 6 mg L^{-1} under WL LED irradiation caused a significant increase in dye removal from 83% to 87% after 12 h, reflecting the influence of substrate concentration on catalytic performance of AgNPs.

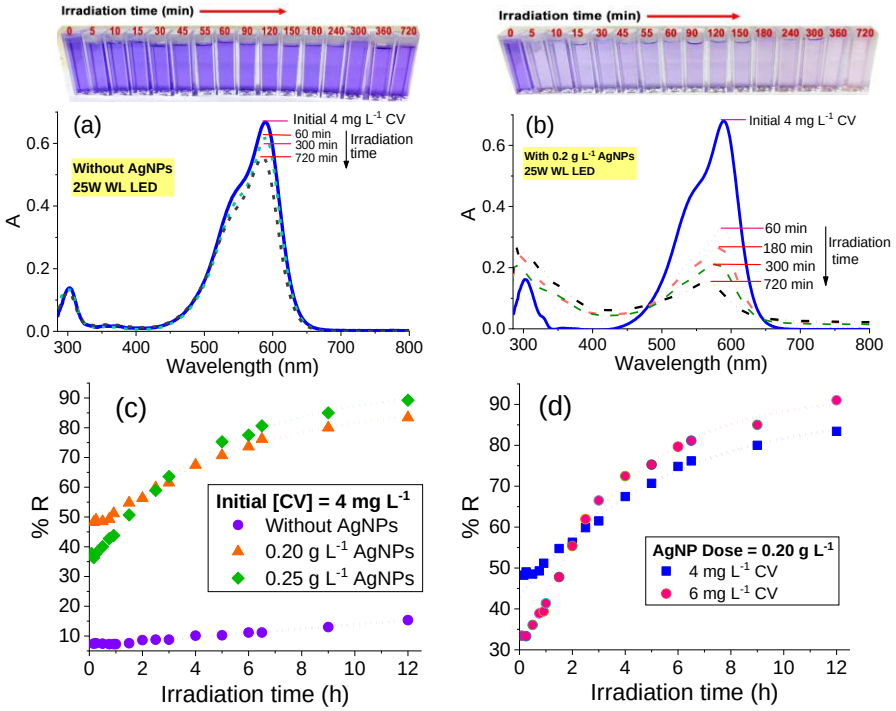

Figure 7 (a - b) UV-Vis spectra and photographs of CV solutions with an initial concentration of 4 mg L^{-1}, irradiated using a 25 W WL LED: (a) without AgNPs and (b) with 0.20 g L^{-1} OW-AgNPs. (c–d) CV removal percentage a function of irradiation time: (c) at different AgNP doses (initial CV concentration fixed at 4 mg L^{-1}) and (d) at two initial CV concentrations (AgNP dose fixed at 0.20 g L^{-1}).

CONCLUSIONS

Silver nanoparticles (AgNPs) were successfully synthesized via a green method using kaffir lime leaf extract (KLLE) as a biogenic reductant and stabilizer. Characterization confirmed the role of flavonoids in nanoparticle formation. Optimal synthesis was achieved at 55ºC using 20 mM $AgNO_3$ and 20% KLLE under neutral pH conditions. The resulting AgNPs (~7.5 nm) exhibited mixed crystalline phases of Ag, AgCl, and Ag_2O, with a total Ag content of ~80 wt%. The KLLE-derived AgNPs demonstrated effective photocatalytic activity for crystal violet (CV) degradation under both white light LED and sunlight, following first-order kinetics with respect to [CV]. Degradation efficiency under white light LED improved with increasing AgNP dose and dye concentration. At an initial [CV] of 4 mg L^{-1} and a catalyst dose of 0.20 g L^{-1}, solar and LED irradiation achieved 85% and 76% CV removal after 6.5 h, respectively. Although continuous 12-h sunlight exposure was impractical due to limited daylight, repeated daily irradiation could potentially enable near-complete degradation.

REFERENCES

Ashkar, M.A., Babu, A., Joseph, R., Kutti Rani, S. and Vasimalai, N. (2023). Ecofriendly synthesis of silver nanoparticles using Radish microgreens extract and their potential photocatalytic degradation of toxic crystal violet and pyronin Y dyes and antibacterial studies. Inorganic Chemistry Communications 156: 111225.

Brandão, A.T., Rosoiu-State, S., Costa, R., Enache, L.B., Mihai, G.V., Vázquez, J.A. and Pereira, C.M. (2025). Unlocking the power of amorphous TiO_2-decorated biocarbon composite: Enhanced photocatalytic performance for crystal violet dye degradation. Journal of Water Process Engineering 71: 107288.

Catauro, M., Papale, F., Bollino, F., Piccolella, S., Marciano, S., Nocera, P., and Pacifico, S. (2015). Silica/quercetin sol-gel hybrids as antioxidant dental implant materials. Science and technology of advanced materials.

Gattuso, G., Barreca, D., Gargiulli, C., Leuzzi, U. and Caristi, C. (2007). Flavonoid composition of citrus juices. Molecules 12(8): 1641 - 1673.

Gebre, S.H. (2023). Bio-inspired synthesis of metal and metal oxide nanoparticles: the key role of phytochemicals. Journal of Cluster Science 34: 665 - 704.

Kanes, K., Tisserat, B., Berhow, M. and Vandercook, C. (1993). Phenolic composition of various tissues of Rutaceae species. Phytochemistry 32(4): 967 - 974.

Kumar, I., Gangwar, C., Yaseen, B., Pandey, P.K., Mishra, S.K. and Naik, R.M. (2022). Kinetic and mechanistic studies of the formation of silver nanoparticles by nicotinamide as a reducing agent. ACS Omega 7(16): 13778 - 13788.

Mandal, K., Das, D., Bose, S.K., Chaudhuri, A., Chakraborty, A., Mandal, S., and Roy, S. (2024). Spectroscopic approach to optimize the biogenic silver nanoparticles for photocatalytic removal of ternary dye mixture and ecotoxicological impact of treated wastewater. Scientific Reports 14(1): 31174.

Marimuthu, S., Antonisamy, A.J., Malayandi, S., Rajendran, K., Tsai, P.C., Pugazhendhi, A. and Ponnusamy, V.K. (2020). Silver nanoparticles in dye effluent treatment: A review on synthesis, treatment methods, mechanisms, photocatalytic degradation, toxic effects and mitigation of toxicity. Journal of Photochemistry and Photobiology B: Biology 205: 111823 (1 - 13).

Mirza, A. and Ahmad, R. (2020). An efficient sequestration of toxic crystal violet dye from aqueous solution by Alginate/Pectin nanocomposite: A novel and ecofriendly adsorbent. Groundwater for Sustainable Development 11: 100373 (1 - 7).

Mushran, S.P., Agrawal, M.C., Mehrotra, R.M. and Sanehi, R. (1974). Kinetics and mechanism of reduction of silver (I) by ascorbic acid. Journal of the Chemical Society, Dalton Transactions 14: 1460 - 1462. Qi, Y., Jiang, M., Cui, Y.L., Zhao, L. and Liu, S. (2015). Novel reduction of Cr(VI) from wastewater using a naturally derived microcapsule loaded with rutin–Cr(III) complex. Journal of Hazardous Materials 285: 336 - 345.

Sahu, N., Soni, D., Chandrashekhar, B., Satpute, D.B., Saravanadevi, S., Sarangi, B.K. and Pandey, R.A. (2016). Synthesis of silver nanoparticles using flavonoids: hesperidin, naringin and diosmin, and their antibacterial effects and cytotoxicity. International Nano Letters 6(3): 173 - 181.

Sana, S.S., Haldhar, R., Parameswaranpillai, J., Chavali, M. and Seong-Cheol Kim. (2022). Silver nanoparticles-based composite for dye removal: A comprehensive review. Cleaner Materials 6: 100161(1 - 14).

Srilatha, D., Nasare, M., Nagasandhya, B., Prasad, V., and Diwan, P. (2013). Development and Validation of UV Spectrophotometric Method for Simultaneous Estimation of Hesperidin and Diosmin in the Pharmaceutical Dosage Form. ISRN Spectroscopy 2013: 534830 (1 - 4).

❑❑❑❑❑